Journal of Solid State Chemistry 186 (2012) 278–282

Contents lists available at SciVerse ScienceDirect

Journal of Solid State Chemistry

journal homepage: www.elsevier.com/locate/jssc

Rapid Communication

Origin of room temperature d^0 ferromagnetism and characteristic photoluminescence in pristine SnO_2 nanowires: A correlation

Gobinda Gopal Khan *, S. Ghosh, Kalyan Mandal

Department of Material Sciences, S.N. Bose National Centre for Basic Sciences, Block JD, Sector III, Salt Lake City, Kolkata 700098, West Bengal, India

ARTICLE INFO

Article history:
Received 28 September 2011
Received in revised form
25 November 2011
Accepted 26 November 2011
Available online 6 December 2011

Keywords:
SnO_2 nanowires
AAO template
d^0 ferromagnetism
Photoluminescence spectroscopy

ABSTRACT

Arrays of SnO_2 nanowires are fabricated by employing a wet chemical template assisted sol–gel route using ordered nanoporous anodic aluminium oxide as the host. The origin of room temperature d^0 ferromagnetism in pristine polycrystalline SnO_2 nanowires is investigated by correlating photoluminescence and electron paramagnetic resonance (EPR) studies. It has been found that the naturally grown structural defects of oxygen vacancies namely singly ionised oxygen vacancy ($V_O^{\bullet}$) clusters induce the characteristic photoluminescence and contribute in ferromagnetism of pristine SnO_2 nanowires at room temperature. The presence of the $V_O^{\bullet}$ structural defects in the pure SnO_2 nanowires is also assured by the EPR spectroscopy. Present study will help understand the puzzle about the unexpected magnetic phenomenon in these undoped wide band gap oxide semiconductors.

1. Introduction

One dimensional (1D) wide band gap oxide semiconductor nanostructures have attracted immense attention due to their potential multifunctional applications in electronics, optoelectronics and spintronics [1–3]. As a wide band gap oxide semiconductor, SnO_2 has been extensively used as a promising candidate to fabricate field effect transistors, photovoltaic devices, optical and sensors systems [4–7]. After the finding of the giant ferromagnetism (FM) in the Co-doped SnO_2 film [8], the transition metal doped SnO_2 has drawn considerable research attention in the area of diluted magnetic semiconductors (DMS) for the probable applications in the spintronics devices. Although room temperature (RT) FM has also been reported in thin films and nanostructures of SnO_2 doped with Co, Fe and Cr [8,9–11], the origin of the RTFM in the DMS always remains controversial, whether it is the intrinsic nature of the semiconductor materials or because of the formation of the secondary phases in the form of ferromagnetic precipitates and metal clusters [12–15]. In order to avoid this controversy the study of the RTFM of the undoped and nonmagnetic ion doped DMS has became very exciting from the perspective of designing new spintronics devices capable of functioning well above the RT. The ferromagnetic response of the undoped and nonmagnetic element doped DMS is called 'd^0 ferromagnetism', as the magnetism is not originated because of the unpaired *d*-orbital electrons [16]. Recently, FM in the undoped SnO_2 nanostructures have been reported [11,17,18], although there is report where SnO_2 nanostructures exhibit diamagnetic response also [19]. The RTFM observed in SnO_2 nanoparticles and nanowires has been demonstrated based on the exchange interactions between localised electron spin moments resulting from oxygen vacancies (V_O, in the Kröger–Vink notation) on the surface [11,17]. Zhang et al. [11] have reported that the FM in SnO_2 nanowires is likely to be due to the surface V_O defects. In case of the undoped oxide semiconductors it is believed that the FM nature is originated because of the different structural defects [20]. For example, point defects can also generate localised moments and mediate FM [21]. In pure oxide semiconductors the most common structural defects are cation vacancies and V_O defects. However, the issue of the origin of RTFM in oxide semiconductors is still not understood properly and hence more in depth investigations are needed to be carried out in order to explain the origin of FM and the physical mechanism behind it.

There are limited recent reports on the RTFM of the pristine SnO_2 nanostructures and still the origin of the FM is lacking proper explanation. In this present work, we report the study of the RTFM in the pristine SnO_2 nanowires (NWs) fabricated by an easy wet chemical template assisted route by using nanoporous anodic aluminium oxide (AAO) as host. The high aspect ratio NWs having large surface to volume ratios are morphologically more advantageous than the nanoparticles in order to obtain long range magnetic ordering. For a pummel understanding of the nature of structural defects present in the pristine SnO_2 NWs, photoluminescence (PL) and electron paramagnetic resonance (EPR) spectroscopy studies are carried out. An interesting strong correlation is found in the experimental results of the PL and EPR studies

* Corresponding author. Fax: +91 33 2335 3477.
E-mail addresses: gobinda@bose.res.in, gobinda.gk@gmail.com (G.G. Khan).

0022-4596/$ - see front matter © 2011 Elsevier Inc. All rights reserved.
doi:10.1016/j.jssc.2011.11.038

with the RTFM, which indicates that the oxygen deficiency related structural defects are responsible for the RTFM in pristine SnO_2 NWs.

2. Experimental methods

The arrays of SnO_2 NWs were synthesised by an easy template assisted route, where the nanoporous AAO template was first fabricated by the controlled two-stage electrochemical anodization of aluminium foil as elaborated in our previous works [22,23]. In brief, highly pure (99.998%) aluminium foil was anodised in a two electrode electrochemical bath maintained at 10 °C using 3 wt% oxalic acid as the electrolyte solution and the anodization was carried out by maintaining a constant current density of 200 A m^{-2} by varying the dc anodization voltage in between 50 and 55 V [22]. The first-stage and the second-stage anodizations were carried out for 20 min and 2 h, respectively. After the first stage anodization the oxide layer was removed by controlled chemical etching and the foil was reanodised for the second time in order to fabricate regularly ordered porous AAO template. The as grown template was dipped inside 10 wt% phosphoric acid solution for 30 min for the opening and rounding of the pore mouths of the nanoporous AAO.

SnO_2 NWs were fabricated within the pores of the AAO by a wet chemical template based sol–gel method reported by Zhu et al. [24]. A solution was prepared by adding 1.2 M urea in a saturated 0.2 M solution of $SnCl_4 \cdot 5\,H_2O$ prepared in ethanol. After the solution was transformed into a transparent sol at RT the AAO template was immersed in the sol and left for four days. The sol containing the template was ultrasonicated several times in order to help the sol to reach inside the pores of the template. After taking the template out from the solution, the sol was removed carefully from its surface and the template was dried under IR source for 20 min. Finally, the arrays of SnO_2 NWs were obtained by annealing the template at 450 °C in air inside a furnace for 2 h.

Field emission scanning electron microscope (FESEM, FEI Helios Nanolab-600) was employed to study the morphology of the as grown SnO_2 NWs by partially removing the AAO template using 2 M NaOH solution. X-ray diffraction (XRD, X'Pert Pro, Panalytical) was used to obtain the crystallographic information of the template embedded SnO_2 NWs. Chemical composition of the NWs was studied by energy dispersive X-ray (EDAX) attached with the FESEM and the inductive coupled plasma (ICP) mass spectroscopy (Varian FT220S). PL measurement of the template embedded NWs was carried out using a spectrofluorometer (Horiba Jobin Yvon, Fluorolog-3) having Xe lamp source. The EPR (Jeol JES-FA100) studies were conducted on the released SnO_2 NWs. Temperature dependent magnetic measurements of the aligned arrays of undoped SnO_2 NWs were carried out using a vibrating sample magnetometer (VSM, Lakeshore, model 7144) in the temperature range of 80–300 K.

3. Results and discussion

3.1. Study of morphology and crystallography

The FESEM micrographs of the arrays of SnO_2 NWs released from the AAO template are shown in Fig. 1(a)–(c). It is clear from the figure that large aspect ratio NWs is prepared in this method. The as grown NWs of uniform diameter are evident from Fig. 1(b) and (c). The diameter of the NWs is about 50 nm, which is found to be very close to the diameter of the pores of the AAO template. The XRD pattern of the as grown pristine SnO_2 NWs, shown in Fig. 1(d), clearly indicates the polycrystalline pure rutile type crystal structure of the NWs (JCPDS card no. 41-1445). The EDAX analysis confirms the formation of SnO_2 NWs within the template indicating the presence of Sn and O only in the NWs. The presence of no other elements as inclusions is detected by the EDAX study. Moreover, the chemical composition of the fabricated NWs analysed by the ICP mass spectroscopy also confirms the formation of pure SnO_2 phase without the presence of any impurity elements, especially transient metal ions in the pristine SnO_2 NWs.

3.2. Photoluminescence study

PL spectroscopy is an exciting tool to investigate the defect-related emissions from the semiconductors. The RT PL emission spectrum of the template embedded SnO_2 NWs is recorded under an excitation of 450 nm light from a Xe lamp is shown in Fig. 2. The AAO template provides a broad blue emission band cantered at 430 nm because of the oxygen vacancy related defects [22]. It is found that the SnO_2 NWs provide luminescence in the green–yellow wavelength region cantered around 520 nm. Generally, SnO_2 nanostructures exhibit emission bands between 450 and 600 nm because of the crystalline defects induced during the growth [25–27]. The Sn vacancies (V_{Sn}) and V_O defects are the main structural defects appeared in the SnO_2 nanostructures during their fabrication and it is believed that they generate trapping states in the band gap leading to luminescence in the visible wavelength region [24]. However, because of the high formation energy of V_{Sn} it is expected that the concentration of the V_{Sn} defects in the pristine SnO_2 should be much lower than that of the V_O defects [28]. In this regard the luminescence from SnO_2 nanostructures in the visible green–yellow wavelength region is ascribed to the V_O related defects [17,19,26,27,29]. These V_O can introduce defect levels situated in the band gap and make a contribution to the mid-gap luminescence activities. Therefore, the green or green–yellow luminescence from the SnO_2 NWs in our experiment is believed to be originated from the trapped state electronic transition related to the V_O defects [17,19]. However, there are three kinds of oxygen vacancy defects namely oxygen vacancies without trapped electron or neutral oxygen vacancies (V_O^X), singly ionised oxygen vacancies ($V_O^{\bullet}$) and doubly ionised oxygen vacancies ($V_O^{\bullet\bullet}$). The symbols are according to the Kröger–Vink notations. As the $V_O^{\bullet\bullet}$ defects introduce very shallow donor state [30], it is expected that the yellow–green visible light emission occurs due to the $V_O^{\bullet}$ acceptor state. Very recently, Kar et al. [31] have elaborately demonstrated the possible luminescence mechanism of the SnO_2 NWs and the studies indicate that the $V_O^{\bullet}$ defects introduces a deep level mid-gap defect state [32] responsible for the yellow–orange luminescence from SnO_2 NWs. Correlating our experimental result with these recent reports, we firmly believe that the characteristics visible green–yellow luminescence from the pristine SnO_2 NWs found in our work is originated from the $V_O^{\bullet}$ defects, most probably situated in the band gap at nearly 2.4 eV above the valence band.

3.3. Electron paramagnetic resonance study

The EPR spectroscopy is an efficient experimental technique to investigate the different kinds of structural defects like V_O defects present in the materials. The as-prepared pure SnO_2 NWs are studied by EPR spectroscopy (see Fig. 3) and by calculating the g factor (EPR parameter) it is possible to get an idea about of the type of V_O defects present using the following equation (Eq. (1)):

$$g = h\gamma/\mu_B H \quad (1)$$

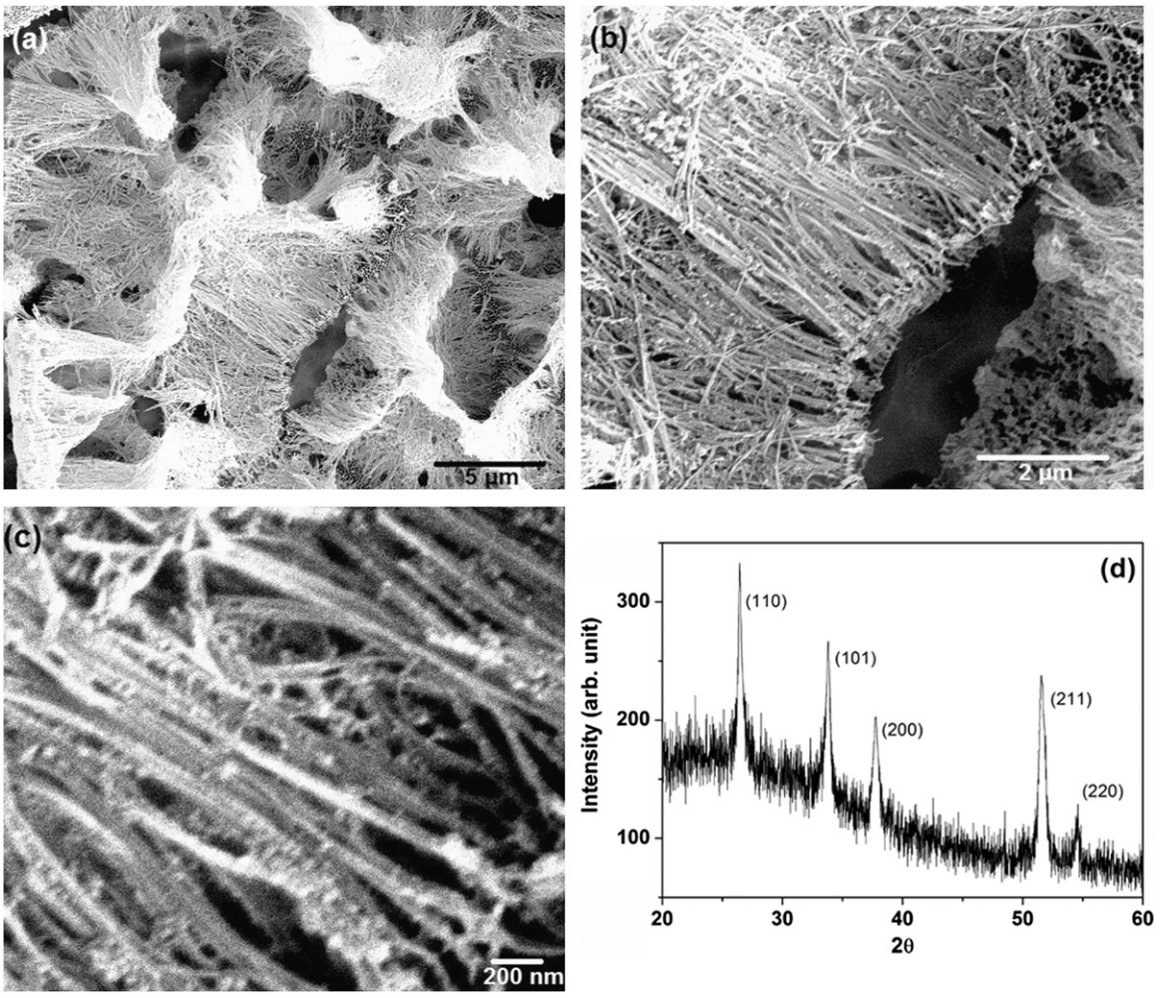

Fig. 1. FESEM micrographs of the as-prepared pure SnO_2 NWs released from the AAO template at different magnifications (a)–(c). (d) XRD pattern of the pure SnO_2 NWs.

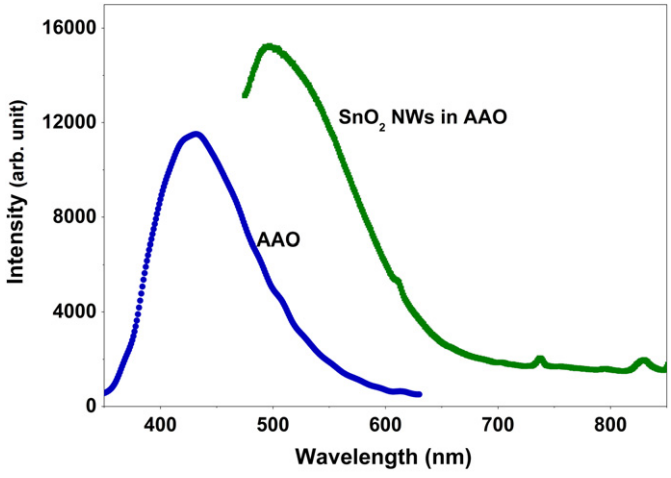

Fig. 2. RT PL spectra of the AAO template and the pure SnO_2 NWs embedded in the AAO template.

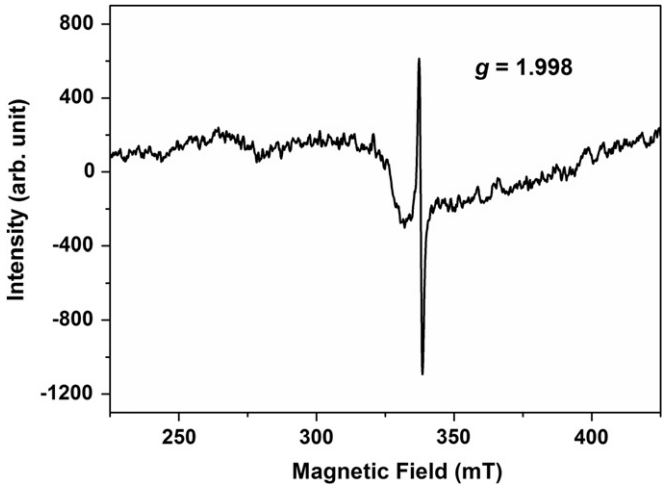

Fig. 3. EPR spectrum of the as-prepared pristine SnO_2 NWs released from the AAO template.

where, H is the magnetic field (gauss), γ is the frequency (Hz), μ_B is the Bohr magnetron equal to 9.274×10^{-21} erg/Gauss and h is Planck's constant, 6.626×10^{-27} erg-s/cycle.

From the above calculation an EPR signal of $g=1.998$ appears from the pure SnO_2 NWs. Recently, Özcan et al. [33] have shown that the Sn^{+4}, Sn^{+2}, V_O^X and $V_O^{\bullet\bullet}$ defect states have an even number of electrons and these are electron spin resonance (ESR)-silent singlets. Furthermore, based on the DFT calculations they also have demonstrated that the g factor around 2.0 can appear because of the $V_O^{\bullet}$ defects in the SnO_2 and this defect is only ESR active [33]. Popescu et al. [34] and Kar et al. [29] have also attributed the ESR signal with the g factor around 2.0 to $V_O^{\bullet}$ defects in the undoped SnO_2 nanostructures. Therefore, our EPR

spectroscopy result with g factor close to 2.0 for the pristine SnO_2 NWs suggests that this signal is originated from the $V_O^{\bullet}$ defects in the NWs, which are believed to be the recombination centres (F^+-type centre) for the luminescence processes [29]. Considerably large concentration of the $V_O^{\bullet}$ luminescent centres present in the SnO_2 NWs is attributed to the visible light emission (trap emission) in the green–yellow region. The EPR study indicates the presence of large concentration of $V_O^{\bullet}$ defects in the pristine SnO_2 NWs fabricated in this work.

3.4. Magnetic property

Fig. 4 shows the room temperature (300 K) hysteresis loops of the as-prepared pure SnO_2 NWs embedded in the AAO template. A clear evidence for FM is observed in the as grown pristine SnO_2 NWs with low saturation magnetic field ($\sim$2000 Oe). In the inset of Fig. 4 the M–H loops of the pristine SnO_2 NWs at 300 and 80 K are shown after subtracting the background diamagnetic signal arising from the AAO template. The RTFM has been reported in the undoped wide band gap semiconductor thin films and nanoparticles like ZnO, TiO_2, CeO_2, SnO_2, In_2O_3 and Al_2O_3, where the origin of the FM is addressed based on the oxygen vacancy defects [17,35,36]. According to Sundaresan et al. [17] the RTFM is a general feature for all the oxide semiconductor nanoparticles and they assumed that this is because of exchange interactions between localised electron spin moments of the oxygen vacancies at the surface of the nanoparticles. For ZnO thin films and nanostructures the Zn vacancies (V_{Zn}) have also been suggested to have localised moment and the cation vacancy defects have been attributed to the ferromagnetic ordering [37]. However, studies show that among the oxygen vacancy defects, the $V_O^{\bullet\bullet}$ centres, which are the shallow donors, form a $1s^2$ singlet state and can only establish weak antiferromagnetic ordering [32]. Coey et al. [32] has reported that the cation vacancies and the adjacent $V_O^{\bullet}$ centres (F^+ centres) or $V_O^{\bullet}$ centre clusters form a triplet state and can initiate defect related hybridisation causing charge transfer from a donor-derived impurity state to the unoccupied states at the Fermi energy level to establish a long-range ferromagnetic interaction. In our work, it is expected that the concentration of the cation vacancy defects (Sn vacancies, V_{Sn}) should be low because of their high formation energy and hence their concentration should be much below the required percolation threshold to mediate long-range ferromagnetic ordering in pristine SnO_2 NWs [19]. In our experiment, we have not also traced the presence of significant amount of Sn vacancies, hence we believe that the $V_O^{\bullet}$ centre defect clusters are responsible for the FM ordering in pure SnO_2 NWs. The presence of the high concentration of the $V_O^{\bullet}$ defects in the SnO_2 NWs fabricated in this work has already been confirmed from the earlier PL and EPR spectroscopy studies. The high concentration of the $V_O^{\bullet}$ centre defects would possibly promote the formation of the $V_O^{\bullet}$ defect clusters (anion vacancy clusters), which can induce magnetisation through the defect band related hybridisation at Fermi level causing localised electron spin moments.

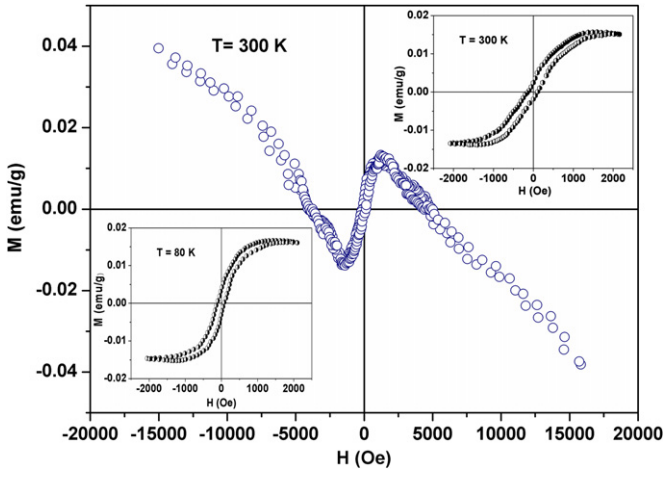

Fig. 4. Magnetic hysteresis loop of the as-prepared pristine SnO_2 NWs measured at 300 K. The insets show the hysteresis loops of pure SnO_2 NWs at 300 and 80 K after subtracting the background diamagnetic signal.

4. Conclusions

In summary, SnO_2 NWs have been successfully fabricated by a facile wet chemical template assisted sol–gel route. The as-prepared pristine SnO_2 NWs exhibit d^0 RTFM. The intense visible green–yellow luminescence and the g factor of 1.998 obtained from the EPR spectroscopy measurement for the pristine SnO_2 NWs suggests the presence of large concentration of $V_O^{\bullet}$ defects. Correlating the PL and EPR spectroscopy results with the RTFM it is believed that the anion vacancy clusters ($V_O^{\bullet}$ defect clusters) are responsible for the significant boost in the ferromagnetic ordering in the pristine SnO_2 NWs. The experimental results also suggest that the sample preparation condition should have an important influence on the optical and magnetic properties of the NWs. By tuning the oxygen vacancy defects in pristine SnO_2 NWs it is possible to control their magnetic and optical properties, which is very exciting from the view point of their successful applications in spintronic and photonic devices.

Acknowledgments

One of the authors (S. G.) thanks Council of Scientific and Industrial Research (CSIR), Government of India, for providing financial support through a research fellowship. The above work is supported by the CSIR funded project 03(1178)/10/EMR-II. The authors also thank Dr. T.K. Paine and Mr. B. Chakraborty of Department of Inorganic Chemistry, Indian Association for the Cultivation of Science, Kolkata, India, for providing the EPR measurement facility.

References

[1] B.A. Buchine, W.L. Hughes, F.L. Degertekin, Z.L. Wang, Nano Lett. 6 (2006) 1155.
[2] J. Bao, M.A. Zimmler, F. Capasso, X. Wang, Z.F. Ren, Nano Lett. 6 (2006) 1719.
[3] I. Žutić, J. Fabian, S. Das Sarma, Rev. Mod. Phys. 76 (2004) 323.
[4] J. Sun, Q. Tang, A. Lu, X. Jiang, Q. Wan, Nanotechnology 20 (2009) 255202.
[5] S. Ferrere, A. Zaban, B.A. Gregg, J. Phys. Chem. B 101 (1997) 4490.
[6] J. Hu, Y. Bando, Q. Liu, D. Golberg, Adv. Funct. Mater. 13 (2003) 493.
[7] X.Y. Xue, Y.J. Chen, Y.G. Liu, S.L. Shi, Y.G. Wang, T.H. Wang, Appl. Phys. Lett. 88 (2006) 201907.
[8] S.B. Ogale, R.J. Choudhary, J.P. Buban, S.E. Lofland, S.R. Shinde, S.N. Kale, V.N. Kulkarni, J. Higgins, C. Lanci, J.R. Simpson, N.D. Browning, S. Das Sarma, H.D. Drew, R.L. Greene, T. Venkatesan, Phys. Rev. Lett. 91 (2003) 077205.
[9] J. Hays, A. Punnoose, R. Baldner, M.H. Engelhard, J. Peloquin, K.M. Reddy, Phys. Rev. B 72 (2005) 075203.
[10] K. Nomura, C.A. Barrero, J. Sakuma, M. Takeda, Phys. Rev. B 75 (2007) 184411.
[11] L. Zhang, S. Ge, Y. Zuo, J. Wang, J. Qi, Scr. Mater. 63 (2010) 953.
[12] S. Ghosh, K. Mandal, J. Magn. Magn. Mater. 322 (2010) 1979.
[13] S. Ghosh, D. De. Munshi, K. Mandal, J. Appl. Phys. 107 (2010) 123919.
[14] S. Ghosh, M. Mandal, K. Mandal, J. Magn. Magn. Mater. 323 (2011) 1083.
[15] A. Zunger, S. Lany, Physics 3 (2010) 53.
[16] S. Ghosh, G.G. Khan, B. Das, K. Mandal, J. Appl. Phys. 109 (2011) 123927.
[17] A. Sundaresan, R. Bhargavi, N. Rangarajan, U. Siddesh, C.N.R. Rao, Phys. Rev. B 74 (2006) 161306(R).
[18] L. Li, K. Yu, Z. Tang, Z. Zhu, Q. Wan, J. Appl. Phys. 107 (2010) 014303.
[19] X. Liu, J. Iqbal, Z. Wu, B. He, R. Yu, J. Phys. Chem. C 4790 (2010) 114.
[20] J. Sakuma, K. Nomura, C. Barrero, M. Takeda, Thin Solid Films 515 (2007) 8653.

[21] G. Rahman, V.M. Garcia-Suarez, S.C. Hong, Phys. Rev. B 78 (2008) 184404.
[22] G.G. Khan, N. Mukherjee, A. Mondal, N.R. Bandyopadhyay, A. Basumallick, Mater. Chem. Phys. 122 (2010) 60.
[23] J. Sarkar, G.G. Khan, A. Basumallick, Bull. Mater. Sci. 30 (2007) 271.
[24] W. Zhu, W. Wang, H. Xu, J. Shi, Mater. Chem. Phys. 99 (2006) 127.
[25] H. He, T.H. Wu, C.L. Hsin, K.M. Li, L.J. Chen, Y.L. Chueh, L.J. Chou, Z.L. Wang, Small 2 (2006) 116.
[26] S. Luo, J. Fan, W. Liu, M. Zhang, Z. Song, C. Lin, X. Wu, P.K. Chu, Nanotechnology 17 (2006) 1695.
[27] S. Luo, P.K. Chu, W. Liu, M. Zhang, C. Lin, Appl. Phys. Lett. 88 (2006) 183112.
[28] C. Kilic, A. Zunger, Phys. Rev. Lett. 88 (2002) 095501.
[29] A. Kar, S. Kundu, A. Patra, J. Phys. Chem. C 118 (2011) 115.
[30] K. Vanheusden, W.L. Warren, C.H. Seager, D.R. Tallant, J.A. Voigt, J. Appl. Phys. 10 (1996) 7983.
[31] A. Kar, M.A. Stroscio, M. Dutta, J. Kumari, M. Meyyappan, Semicond. Sci. Technol. 25 (2010) 024012.
[32] J.M.D. Coey, M. Venkatesan, C.B. Fitzgerald, Nature Mater. 4 (2005) 173.
[33] N. Özcan, T. Kortelainen, V. Golovanov, T.T. Rantala, J. Vaara, Phys. Rev. B 81 (2010) 235202.
[34] D.A. Popescu, J.M. Herrmann, A. Ensuque, F. Bozon-Verduraz, Phys. Chem. Chem. Phys. 3 (2001) 2522.
[35] X. Wei, R. Skomski, B. Balamurugan, Z.G. Sun, S. Ducharme, D.J. Sellmyer, J. Appl.Phys. 105 (2009) 07C517.
[36] R. Podila, W. Queen, A. Nath, J.T. Arantes, A.L. Schoenhalz, A. Fazzio, G.M. Dalpian, J. He, S.J. Hwu, M.J. Skove, A.M. Rao, Nano Lett. 10 (2010) 1383.
[37] Q. Wang, Q. Sun, G. Chen, Y. Kawazoe, P. Jena, Phys Rev. B 77 (2008) 205411.